Time-history influence of global dust storms on the upper atmosphere at Mars

Michael W. Liemohn,[1] Ava Dupre,[1] Stephen W. Bougher,[1] Matthew Trantham,[1] David L. Mitchell,[2] and Michael D. Smith[3]

Received 10 April 2012; revised 3 May 2012; accepted 4 May 2012; published 2 June 2012.

[1] A recent survey of the Mars Global Surveyor (MGS) electron data for dayside photoelectron observations over regions of strong crustal fields revealed an unusual bimodal solar flux dependence. The elevated-flux population was associated with the timing of a large global dust storm in late 2001. The results of a systematic study parameterizing the photoelectron flux intensities against a solar flux proxy and MGS-observed atmospheric dust opacity are presented here. Instantaneous dust opacities were used as well as time-history averages and maximal values. The result is a functional form for the photoelectron fluxes against these parameters. The inclusion of instantaneous dust opacity values in the function do not improve the correlation, but a time-history window significantly enhances the correlation and explains the bimodal distribution in the electron fluxes. The best relationship was obtained with 7-Earth-month time-history dust opacity variables included in the function. The most likely explanation for this long-lived influence of dust storms is a composition and/or density change in the upper atmosphere. **Citation:** Liemohn, M. W., A. Dupre, S. W. Bougher, M. Trantham, D. L. Mitchell, and M. D. Smith (2012), Time-history influence of global dust storms on the upper atmosphere at Mars, *Geophys. Res. Lett.*, *39*, L11201, doi:10.1029/2012GL051994.

1. Introduction

[2] *Trantham et al.* [2011] conducted a systematic analysis of photoelectron fluxes in the dayside ionosphere of Mars. By carefully isolating the dayside photoelectron flux signature [see, e.g., *Mantas and Hanson*, 1979] in the magnetometer/electron reflectometer (MAG/ER) data from Mars Global Surveyor (MGS) [*Acuña et al.*, 1992; *Mitchell et al.*, 2001], and by focusing on the mapping and extended mission phases when MGS was in a ∼400 km altitude circular, sun-synchronous orbit, they were able to quantify the factors controlling the flux intensities of these particles. While they found that the local solar EUV proxy was the defining controlling factor for the photoelectron intensity, they also found a dual linear trend in this dependence. Specifically, they found that the period of late 2001 and early 2002 has an elevated linear relationship, with an increase in both slope and intercept, for the photoelectron flux dependence on the local solar EUV intensity.

[3] The timing of the enhanced electron flux population coincides with a large global dust storm at Mars [e.g., *Smith et al.*, 2002]. Dust storms typically occur on Mars in the southern spring, when Mars is near perihelion along its eccentric orbit about the Sun. This dust radiatively heats the lower atmosphere of Mars as the particles absorb visible solar photons and planetary infrared photons, to the point of significantly suppressing the formation of water clouds in the lower atmosphere [e.g., *Pearl et al.*, 2001; *Smith*, 2002].

[4] The influence of lower atmosphere dust storms and seasonally variable dust opacities have been observed in various thermospheric observations [e.g. *Keating et al.*, 1998; *Bougher et al.* 1999, 2004, 2006; *Baird et al.*, 2007; *Lillis et al.*, 2008, 2010]. The influence of dust storms has even been recorded in ionospheric electron densities [*Wang and Nielsen*, 2003]. Using coupled lower and upper atmosphere global circulation models, *Bougher et al.* [1997] found a 5–10 times increase in thermospheric density at 110 km for a sample 20 SOL dust storm event, along with a ∼20 K cooling of the thermosphere above the dust storm (due to upwelling) and a 20–50 K warming of the thermosphere in the North polar region (due to downwelling) owing to adiabatic expansion (cooling) and contraction (heating) from the time evolving upper atmosphere circulation. *Bougher et al.* [2006] expanded upon this study with a systematic investigation of the impacts of lower atmosphere seasonally variable dust heating on the thermospheric temperatures and wind structure, quantifying the changes up to 200 km altitude.

[5] Observationally, the results are mixed. *Keating et al.* [1998] noted a 200% (factor of 3) increase in mass density from MGS accelerometer data a few days after the start of a dust storm at the 130 km altitude periapsis during aerobraking. From MGS data during the science phasing orbits, *Tracadas et al.* [2001] found a 100% increase (factor of 2) increase in mass density at 180 km about 7 days after the start of a regional dust storm in the opposite hemisphere. The MGS observations are at 400 km altitude, however, far above the peak production layer in the ionosphere. *Forbes et al.* [2008] conducted a systematic investigation of the orbital information from MGS (and deviations from orbit determination techniques) during the mapping and extended mission phases. Interestingly, the variations in the exospheric density (and inferred temperature) at MGS could be adequately

[1]Atmospheric, Oceanic, and Space Sciences Department, University of Michigan, Ann Arbor, Michigan, USA.
[2]Space Sciences Laboratory, University of California, Berkeley, California, USA.
[3]NASA Goddard Spaceflight Center, Greenbelt, Maryland, USA.

Corresponding author: M. W. Liemohn, Atmospheric, Oceanic, and Space Sciences Department, University of Michigan, 2455 Hayward St., Ann Arbor, MI 48109-2143, USA. (liemohn@umich.edu)

0094-8276/12/2012GL051994

parameterized by the 81-day mean F10.7 value at Mars. The addition of dust opacity into the formulation made no significant improvement on the fit.

[6] The findings of the study of *Forbes et al.* [2008] and the photoelectron study of *Trantham et al.* [2011] seem to be at odds with each other. A logical next step to the *Trantham et al.* [2011] analysis is the inclusion of dust opacity in the controlling factors for determining the linear functional dependence of photoelectron intensity at 400 km altitude. The optical depth of dust in the atmosphere can be determined from measurements of the Thermal Emission Spectrometer (TES) onboard MGS [*Christensen et al.*, 1992; *Smith*, 2004]. The study presented below uses this additional data set to quantify the influence of dust on Mars dayside photoelectron fluxes.

2. Observations

[7] The MAG/ER instrument on MGS is fully described by *Acuña et al.* [1992], and *Trantham et al.* [2011] presented a methodology for isolating the dayside photoelectron fluxes in the MGS MAG/ER dataset. The identification of this electron population in the ER observations concentrated on the region of strong crustal field lines, located near 180° longitude in the southern hemisphere [*Acuña et al.*, 1998]. Both a spatial constraint (a specific latitude-longitude box) and a magnetic field magnitude minimum constraint were applied to select the strong crustal field region. The removal of measurements of precipitating solar wind electrons was achieved by only considering magnetic field elevations with 45° of horizontal and using only the dayside half of the MGS orbit (solar zenith angle less than 90°). The elevation angle criterion was determined after a careful inspection of the ER dataset for the occurrence of precipitating solar wind electrons; within the envelope of the other criteria, elevation angles within 45° of horizontal are absolutely clear of solar wind electrons and contain only photoelectron spectra. This produced ~280,000 electron velocity space samples over the 6+ Earth-years of the mapping and extended mission phases of MGS.

[8] The details of the TES instrument on MGS are given by *Christensen et al.* [1992, 2001], and the method of extracting dust opacity values from these observations is presented in detail by *Smith* [2004]. In short, the spectral dependence of radiance observed by TES in the 15-micron CO_2 band is first used to retrieve an atmospheric temperature profile, and then the rest of the TES spectrum is fit using a radiative transfer model to retrieve the column abundance of water vapor and the column optical depth of dust and water ice aerosol.

[9] Figure 1 shows a time series of various quantities of relevance during the mapping and extended mission phases of MGS. Shown are the MGS ER photoelectron fluxes in the 27 eV energy channel and 90° pitch angle bin [*Trantham et al.*, 2011], along with a Mars solar EUV proxy [*Mitchell et al.*, 2001], the local solar zenith angle, the latitude-dependent MGS TES dust opacity optical depths, and various time series compilations of this dust opacity. The 2-year periodic fluctuation in the photoelectron fluxes and the solar EUV proxy are from the eccentricity of the Mars orbit, which varies from 1.38 to 1.67 AU distance from the Sun. This same trend is also seen in the TES dust opacity values, as regional and global dust storms typically occur near perihelion during southern hemisphere spring. Qualitatively examining the timing of the peaks and troughs in these time series data, it appears that they all trend together to a large degree.

3. Results

[10] These values were used with the local solar EUV flux proxy to create a new controlling function to specify the photoelectron flux observations. Figure 2 shows scatter plots of 27 eV photoelectron fluxes against various forms of these controlling functions. Table 1 defines the quantities used for the x-axis values in Figure 2. Also shown in each of the panels of Figure 2 are asterisk symbols showing the median and quartiles (as error bars) for all of the data points within 10 equally spaced bins. A linear fit to these median values is show as a red line, with the slope and intercept quantities for this fit given in the lower right corner. Correlation coefficients (given in the below) are for the entire data set.

[11] The Pearson correlation coefficient (R) with no TES dust opacity in the function (Figure 2a) is 0.30 (final column in Table 1). Because the scatterplot contains over 280,000 data points, this is well above the mathematical definition of statistical significance. The double linear trend is clearly seen in Figure 2a. The inclusion of the dust opacity at the latitude of the photoelectron observation as a multiplier in the x-axis controlling function definition (Figure 2b) does not change the overall pattern of the data. Similarly, the inclusion of the global dust opacity in the function (Figure 2c) still shows a distinct difference in the photoelectron populations. In fact, Figures 2a–2c have very comparable correlation coefficients (see Table 1). These results are contrasted with Figure 2d, which is based on a 7-Earth-month time-history window to obtain a running average of the globally-averaged dust opacity values. This dust time series was then used as a multiplier of the solar EUV proxy in the controlling function. Unlike the other plots in Figure 2, Figure 2d (and Figure 2e, based on a maximum value within a time-history window) no longer has the double linear trend but rather a single linear trend for the entire photoelectron data set.

[12] The results were not that sensitive to the exact length of this time-history window. To illustrate this, Figure 3 shows R as a function of window length, from the instantaneous globally-averaged values (a window length of zero) to an entire Earth year. The R value increases and then gradually peaks at the 210-Earth-day window length for both the running average and the maximal time-history values in the controlling function. The correlation then worsens with increasing window length, but not by much. It is seen in Figure 3 that the use of a running average versus a maximal value from the interval does not appreciably change the correlation coefficient.

[13] In addition, the results were not improved by using a linear combination of various TES dust values. For example, combining the instantaneous global dust opacity with a time-history maximal value did not raise the best R value, and usually lowered R for a large proportion of the instantaneous value. Finally, other pitch angles and energies of the electron distribution were examined, revealing similar dual linear dependencies with solar EUV and a conversion of this

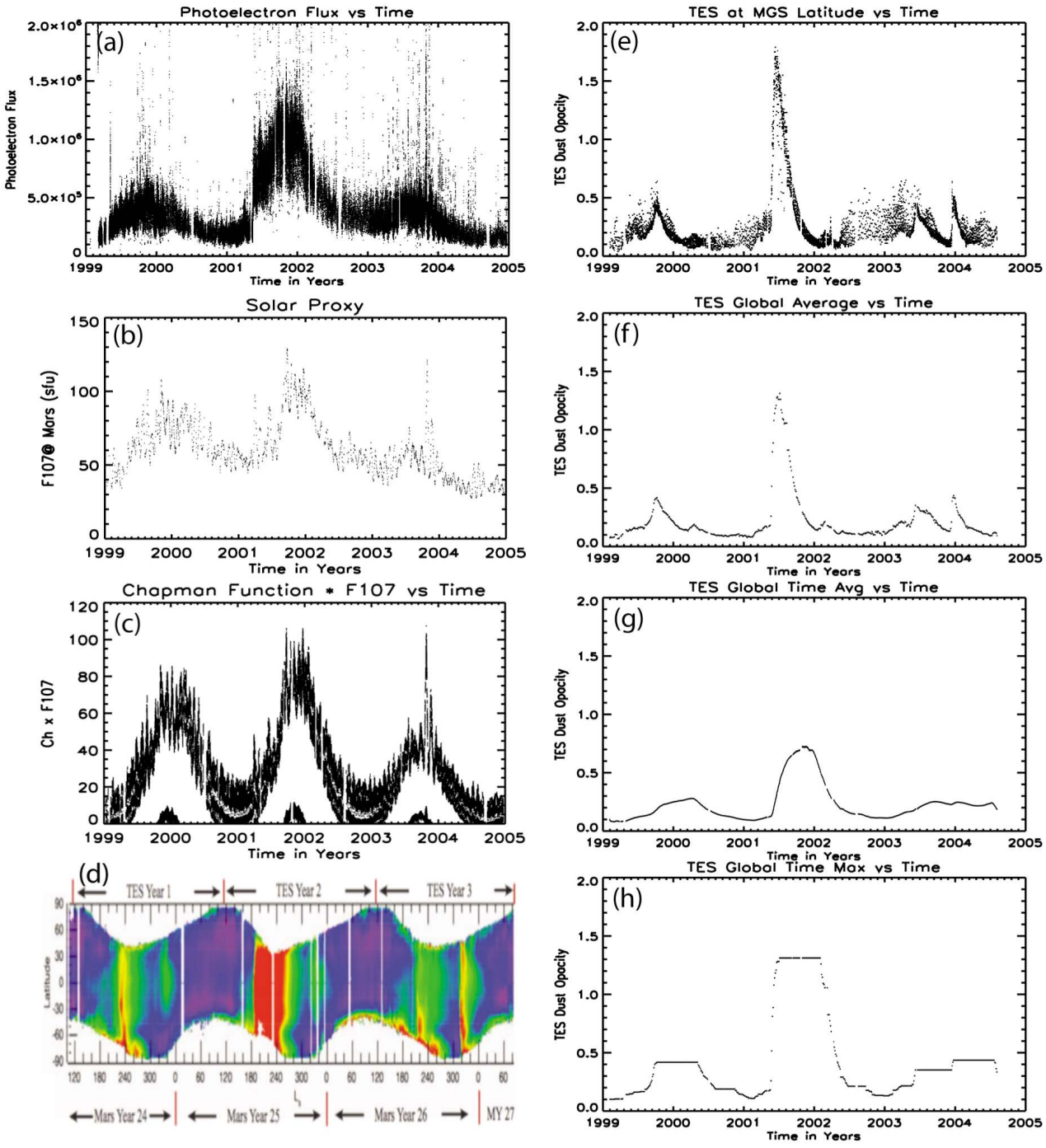

Figure 1. Time series of data over the MGS mapping and extended mission phases. (a) MGS ER photoelectron fluxes in the 27 eV energy channel and 90° pitch angle bin. (b) Solar EUV proxy for Mars, (c) Local solar flux proxy assuming a Chapman function solar zenith angle dependence. (d) MGS TES dust opacity optical depths versus latitude in the mapping and extended mission phases [*McDunn et al.*, 2010]. (e) Dust opacities at the time and place of the photoelectron measurements. (f) Globally-averaged dust opacities. (g) Time-history averages of dust opacity with a 7-Earth-month window. (h) Time-history maximum dust values with a 7-Earth-month window.

double trend into a single linear trend with the inclusion of a time-history dust factor in the controlling function.

4. Discussion

[14] The results presented above show that dust storms at Mars have a long-lasting influence on the photoelectron fluxes at 400 km altitude, well above the source region of these particles (which is in the 100–200 km range). Furthermore, this analysis is done on the 90° pitch angle bin in the MAG/ER dataset. That is, this study presents observations of locally-mirroring electrons that do not have direct access to the source region and exist because of high-altitude

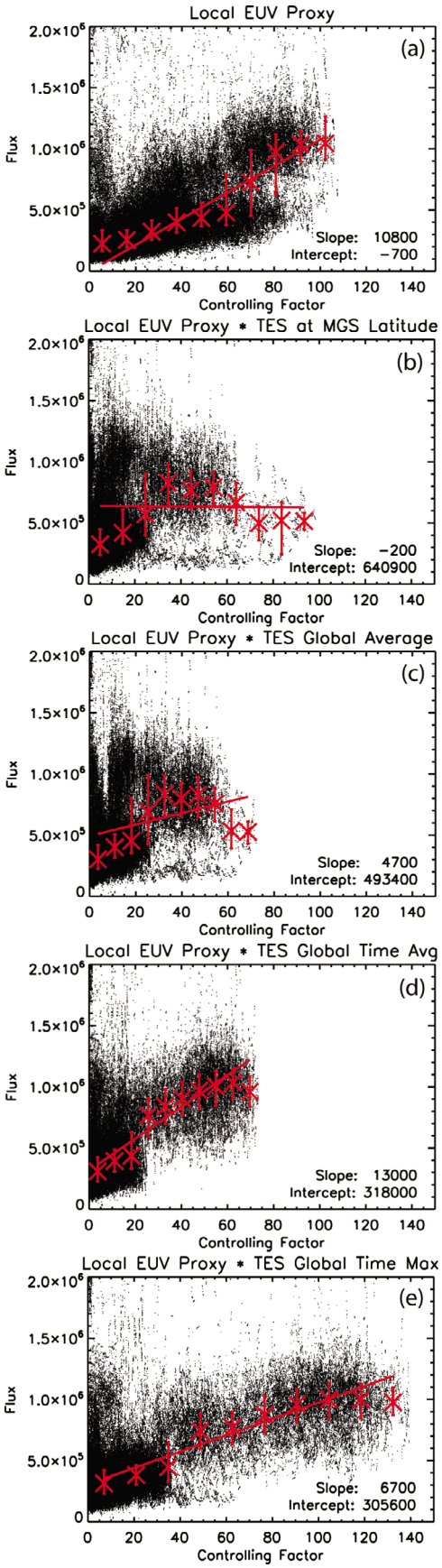

Figure 2. Scatter plots of photoelectron fluxes versus a controlling function as defined by (a) local solar EUV proxy, (b) solar EUV proxy times the instantaneous dust opacity value at the latitude of the photoelectron observation, (c) solar EUV proxy times the instantaneous globally-averaged dust opacity, (d) solar EUV proxy times the 7-Earth-month time history running average of global dust opacity, and (e) solar EUV proxy times the 7-Earth-month time history maximum value of global dust opacity. The asterisks show medians and quartiles for 10 equally-spaced bins and the red line is a linear fit to these median values (with slope and intercept given in the lower right).

Table 1. Photoelectron Flux Controlling Function Parameters

Figure	X-Axis Value Factors	Figures for Input Data	R
2a	(Solar EUV proxy)*(Chapman function of local position)	1c	0.30
2b	(Local EUV)*(Dust Opacity @ MGS Lat. and time)	1c*1e	0.27
2c	(Local EUV)*(Globally-Averaged Opacity @ MGS time)	1c*1f	0.32
2d	(Local EUV)*(Global Opacity averaged over last 7 months)	1c*1g	0.44
2e	(LocalEUV)*(Global Opacity maximum over last 7 months)	1c*1h	0.46

scattering into the mini-magnetospheric magnetic bottle along these field lines. Therefore, this finding implies that the dust storm is altering not only the thermospheric source region of the photoelectrons but also the exospheric neutral particles responsible for the infrequent collisions that fill the trapped zone. This appears to be in direct conflict with the conclusion of *Forbes et al.* [2008], who found that dust opacity has no significant influence on the density or temperature at the MGS mapping/extended phase altitude.

[15] The main argument for consistency rather than conflict in the different MGS data set analyses is that all of the previous studies (mentioned in the Introduction section above) address only the instantaneous dust opacity connection with the upper atmosphere, and none specifically deals with the question of time-history influences of global dust storms. All of these papers imply or assume that the response subsides with the time evolution of the dust storm, and none considered the use of a time-history window to identify a long-term influence on the upper atmosphere. This lack of a strong connection with instantaneous dust opacities was also found in the present study.

[16] Furthermore, the *Forbes et al.* [2008] used near-equatorial dust opacities averaged between $\pm 30^{\circ}$ latitude, while the present study uses globally-averaged dust opacities. This difference means that *Forbes et al.* [2008] minimized the influence of regional dust storms in their analysis, but their influence is greater in the present analysis. This could account for a difference in response functions.

[17] Note that photoelectrons do not last more than a single day in the Mars upper atmosphere, recombining on the nightside to the point that the closed crustal field lines are observed to be plasma voids [*Mitchell et al.*, 2001]. This means that the long-lived influence must be due to perturbations in the neutral atmosphere (in the source region and/or

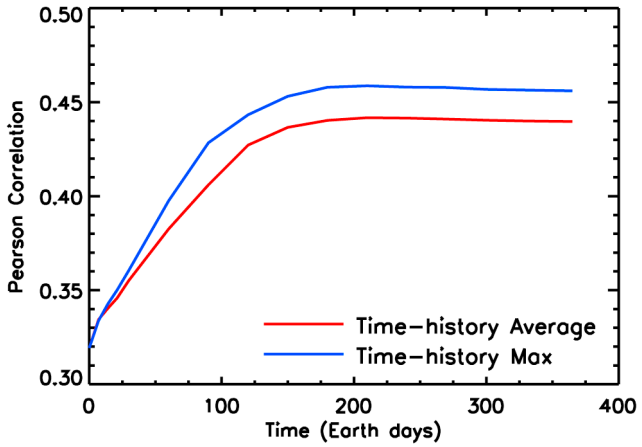

Figure 3. Correlation coefficient of photoelectron fluxes versus a controlling function produced by the local solar EUV proxy times a time-history interval of various Earth-day window lengths, shown for a running-average dust opacity factor (red curve) and a maximum-value dust opacity factor (blue curve).

the high-altitude scattering region). A possible mechanism for a long-lived influence is that the composition of Mars' thermosphere/exosphere might experience long-term changes after a large dust storm (rather than the total density, as monitored by *Forbes et al.* [2008]). That is, if a minor constituent of the Mars upper atmosphere was preferentially enhanced relative to the dominant species, then the photoelectrons could be experiencing an elevated intensity and/or high altitude scattering rate without a noticeable change in the total neutral density. It is the neutral particle densities at and above the MGS orbit of ~400 km altitude that cause the pitch-angle scattering of the electrons to get them to 90° pitch angle at the spacecraft altitude. The two likely suspects for this are atomic oxygen and hydrogen, which dominate at high altitudes but not in the photoelectron source region of the thermosphere. This is possible because the upper thermospheric neutral processes are species specific, and therefore the density of each species can independently vary. The exospheric density above the MGS orbit altitude, where these two species dominate the neutral composition, would therefore significantly increase.

[18] The question arises as to why these species would be preferentially elevated for months after a global dust storm subsides. One explanation is that the collision frequency in the exosphere is very low and lifetimes of planet-orbiting particles are relatively long. Therefore, transient changes to the exobase composition might linger in the high-altitude space above Mars for an extended period of time. *Valeille et al.* [2009] found that the atomic oxygen exospheric density changes by 20% over a season. This is partly from long-lived particles on orbital (rather than ballistic) trajectories. A dust-induced increase could also be long-lived and of this magnitude due to these orbiting neutrals. Another is that some dynamical process in the lower atmosphere could be systematically altered to produce a long-lasting forcing on the bottom side of the thermosphere. For instance, planetary waves and tides are perturbed by the dust storm and could have a very slow damping rate, allowing for a long-term influence. Yet another mechanism could be a chemical composition change in the lower atmosphere due to the storms that then propagates upward, slowly influencing the thermosphere over an extended period. A final possibility to be mentioned here is a lingering influence of very small dust grains, below the detection threshold of TES. Specifically, if any of these lower atmospheric possibilities led to an enhanced Eddy diffusion coefficient (Kzz), the mixed lower atmosphere would become deeper and the homopause would shift upward. This would especially influence the minor light species (like H and O) because vertical molecular diffusion would then take control at a higher altitude. The impact of even a small increase in Kzz would be a larger light species distribution in the upper thermosphere and exosphere. This could lead to long-lasting yet difficult-to-detect change in the upper atmosphere. An investigation of which of these possibilities is responsible for the time-history effect seen in the MGS photoelectron data is left for a future study.

5. Conclusions

[19] A survey of photoelectrons at Mars revealed a bimodal relationship with solar EUV flux, the timing of which was related to a strong global dust storm. It was determined that the inclusion of the instantaneous dust opacity (local or globally averaged) in the photoelectron flux dependency function did not improve the correlation coefficient. However, the use of a time-history dust opacity value in the formula greatly improves the correlation coefficient. The best correlation was found with a 210-Earth-day window, but peak in R is not sharp and a broad range of time-history windows yielded similarly good correlations. The best-fit function completely explains the dual linear distribution of the photoelectron fluxes by shifting the upper linear trend over in line with the end of the lower linear trend.

[20] A possible mechanism for creating this long-term influence is a composition change in the thermosphere and exosphere, specifically of some minor species that significantly contributes to the density at altitudes above the MGS orbit. Likely candidates are atomic oxygen or hydrogen, which could be enhanced by one or more of several physical processes. Regardless of the physical process, this study suggests a need to take into account the time-history of dust when considering the dynamics and chemistry of the upper atmosphere.

[21] **Acknowledgments.** The authors thank NASA and NSF for supporting this work, particularly under NASA grants NNX07AN98G and NNX11AD80G and NSF grant AST-0908311.

[22] The Editor thanks two anonymous reviewers for assisting in the evaluation of this paper.

References

Acuña, M. H., et al. (1992), Mars Observer magnetic fields investigation, *J. Geophys. Res.*, *97*, 7799–7814, doi:10.1029/92JE00344.

Acuña, M. H., et al. (1998), Magnetic field and plasma observations at Mars: Initial results of the Mars Global Surveyor Mission, *Science*, *279*, 1676–1676, doi:10.1126/science.279.5357.1676.

Baird, D. T., R. Tolson, S. W. Bougher, and B. Steers (2007), Zonal wind calculation from MGS accelerometer and rate data, *J. Spacecr. Rockets*, *44*(6), 1180–1187, doi:10.2514/1.28588.

Bougher, S. W., J. Murphy, and R. M. Haberle (1997), Dust storm impacts on the Mars upper atmosphere, *Adv. Space Res.*, *19*(8), 1255–1260, doi:10.1016/S0273-1177(97)00278-0.

Bougher, S. W., G. M. Keating, R. W. Zurek, J. M. Murphy, R. M. Haberle, J. Hollingsworth, and R. T. Clancy (1999), Mars Global Surveyor aerobraking: Atmospheric trends and model interpretation, *Adv. Space Res.*, *23*(11), 1887–1897, doi:10.1016/S0273-1177(99)00272-0.

Bougher, S. W., S. Engel, D. P. Hinson, and J. R. Murphy (2004), MGS Radio Science electron density profiles: Interannual variability and implications for the Martian neutral atmosphere, *J. Geophys. Res.*, *109*, E03010, doi:10.1029/2003JE002154.

Bougher, S. W., J. M. Bell, J. R. Murphy, M. A. Lopez-Valverde, and P. G. Withers (2006), Polar warming in the Mars thermosphere: Seasonal variations owing to changing insolation and dust distributions, *Geophys. Res. Lett.*, *33*, L02203, doi:10.1029/2005GL024059.

Christensen, P. R., et al. (1992), Thermal Emission Spectrometer Experiment: Mars Observer mission, *J. Geophys. Res.*, *97*, 7719–7734, doi:10.1029/92JE00453.

Christensen, P. R., et al. (2001), Mars Global Surveyor Thermal Emission Spectrometer experiment: Investigation description and surface science results, *J. Geophys. Res.*, *106*, 23,823–23,871, doi:10.1029/2000JE001370.

Forbes, J. M., F. G. Lemoine, S. L. Bruinsma, M. D. Smith, and X. Zhang (2008), Solar flux variability of Mars' exosphere densities and temperatures, *Geophys. Res. Lett.*, *35*, L01201, doi:10.1029/2007GL031904.

Keating, G. M., et al. (1998), The structure of the upper atmosphere of Mars: In situ accelerometer measurements from Mars Global Surveyor, *Science*, *279*, 1672–1676, doi:10.1126/science.279.5357.1672.

Lillis, R. J., S. W. Bougher, D. L. Mitchell, D. A. Brain, R. P. Lin, and M. H. Acuña (2008), Continuous monitoring of nightside upper thermospheric mass densities in the Martian southern hemisphere over 4 Martian years using electron reflectometry, *Icarus*, *194*, 562–574, doi:10.1016/j.icarus.2007.09.031.

Lillis, R. J., S. W. Bougher, F. González-Galindo, F. Forget, M. D. Smith, and P. C. Chamberlin (2010), Four Martian years of nightside upper thermospheric mass densities derived from electron reflectometry: Method extension and comparison with GCM simulations, *J. Geophys. Res.*, *115*, E07014, doi:10.1029/2009JE003529.

Mantas, G. P., and W. B. Hanson (1979), Photoelectron fluxes in the Martian ionosphere, *J. Geophys. Res.*, *84*, 369–385, doi:10.1029/JA084iA02p00369.

McDunn, T., S. W. Bougher, J. Murphy, M. D. Smith, F. Forget, J.-L. Bertaux, and F. Montmessin (2010), Simulating the density and thermal structure of the middle atmosphere (~80–130 km) of Mars using the MGCM-MTGCM: A comparison with MEX-SPICAM observations, *Icarus*, *206*, 5–17, doi:10.1016/j.icarus.2009.06.034.

Mitchell, D. L., R. P. Lin, C. Mazelle, H. Rème, P. A. Cloutier, J. E. P. Connerney, M. H. Acuna, and N. F. Ness (2001), Probing Mars' crustal magnetic field and ionosphere with the MGS Electron Reflectometer, *J. Geophys. Res.*, *106*(E10), 23,419–23,427, doi:10.1029/2000JE001435.

Pearl, J. C., M. D. Smith, B. J. Conrath, J. L. Bandfield, and P. R. Christensen (2001), Observations of Martian ice clouds by the Mars Global Surveyor Thermal Emission Spectrometer: The first Martian year, *J. Geophys. Res.*, *106*(E6), 12,325–12,338, doi:10.1029/1999JE001233.

Smith, M. D. (2002), The annual cycle of water vapor on Mars as observed by the Thermal Emission Spectrometer, *J. Geophys. Res.*, *107*(E11), 5115, doi:10.1029/2001JE001522.

Smith, M. D. (2004), Interannual variability in TES atmospheric observations of Mars during 1999–2003, *Icarus*, *167*, 148–165, doi:10.1016/j.icarus.2003.09.010.

Smith, M. D., B. J. Conrath, J. C. Pearl, and P. R. Christensen (2002), Thermal Emission Spectrometer observations of Martian planet-encircling dust storm 2001A, *Icarus*, *157*, 259–263, doi:10.1006/icar.2001.6797.

Tracadas, P. W., M. T. Zuber, D. E. Smith, and F. G. Lemoine (2001), Density structure of the upper thermosphere of Mars from measurements of the air drag on the Mars Global Surveyor spacecraft, *J. Geophys. Res.*, *106*, 23,349–23,357, doi:10.1029/2000JE001418.

Trantham, M., M. W. Liemohn, D. L. Mitchell, and J. Frank (2011), Photoelectrons on closed crustal field lines at Mars, *J. Geophys. Res.*, *116*, A07311, doi:10.1029/2010JA016231.

Valeille, A., M. R. Combi, S. W. Bougher, V. Tenishev, and A. F. Nagy (2009), Three-dimensional study of Mars upper thermosphere/ionosphere and hot oxygen corona: 2. Solar cycle, seasonal variations, and evolution over history, *J. Geophys. Res.*, *114*, E11006, doi:10.1029/2009JE003389.

Wang, J.-S., and E. Nielsen (2003), Behavior of the Martian dayside electron density peak during global dust storms, *Planet. Space Sci.*, *51*, 329–338, doi:10.1016/S0032-0633(03)00015-1.